

Article

Full Surface Heat Transfer Characteristics of Stator Ventilation Duct of a Turbine Generator

Shinyoung Jeon ¹, Changmin Son ^{2,*} and Jangsik Yang ¹¹ Pusan National University; Shinyoung.jeon@pusan.ac.kr² Virginia Polytechnic Institute and State University; changminson@vt.edu

* Correspondence: changminson@vt.edu; Tel.: +1-540-235-6010

Received: date; Accepted: date; Published: date

Abstract: Turbine generator operates with complex cooling system due to the challenge in controlling the peak temperature of the stator bar caused by ohm loss, which is unavoidable. Therefore, it is important to characterize and quantifies the thermal performance of the cooling system. The focus of the present research is to investigate the heat transfer and pressure loss characteristics of typical cooling system, so-called stator ventilation duct. A real scale model was built at its operating conditions for the present study. The direction of cooling air is varied to consider its operation condition, so that there are (1) outward flow and (2) inward flow cases. In addition, the effect of (3) cross flow (inward with cross flow case) is also studied. The transient heat transfer method using thermochromic liquid crystals is implemented to measure full surface heat transfer distribution. A series of Computational Fluid Dynamics analysis is also conducted to support the observation from the experiment. For the inward flow case, the results suggest that the average Nusselt number of the 2nd duct is about 30% higher than the 3rd duct. The trend is similar with the effect of cross flow. The CFD results are in good agreement with the experimental data.

Keywords: turbo generator; stator ventilation duct; transient heat transfer; pressure loss

1. Introduction

The increasing demand for electric energy drives the need of bigger power generation system, in general. It continuously requires large capacity turbine generator with higher efficiency. The turbine generator is simple in its principle but is also a very complicate machine to meet the requirements for performance and reliability. One of the key challenges is to control the peak temperature of the generator caused by ohm loss, which is unavoidable. The peak temperature of a generator should be maintained below 130°C, typically.

Figure 1 shows the typical cooling system of a turbine generator. Cooling air pumped by a fan feeds into rotor ventilation duct and the spent air (hotter) mixes with the air through stator ventilation ducts in the air gap. The stator cooling circuit consist of radially inward and outward flows, while the rotor only implements radially outward flow cooling. For the complex cooling system implemented for the turbine generator, it is important to characterize and quantifies the heat transfer and pressure loss to maintain its performance and reliability.

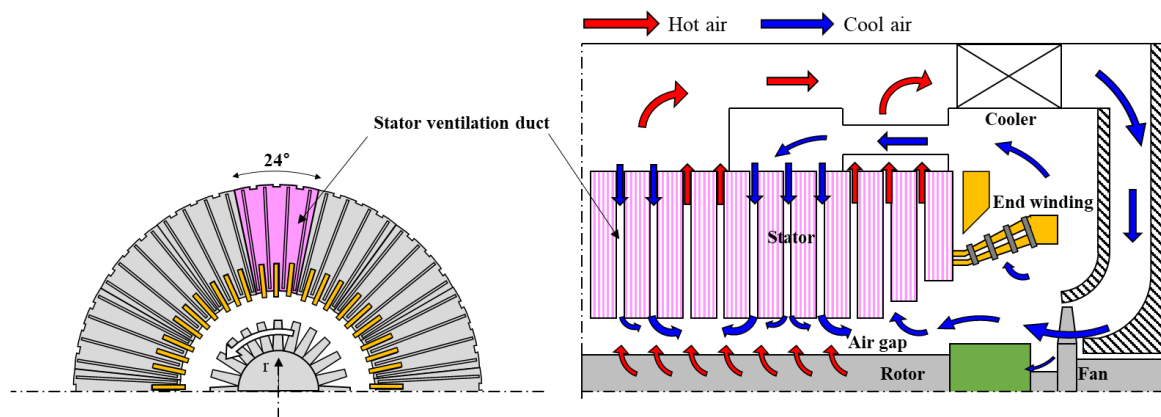


Figure 1. Cooling system of turbine generator and cooling system circuit

There was much effort to investigate the complex cooling system of turbine generator. Yoo et al., [1] reported the detail heat transfer and pressure loss characteristics of rotor ventilation duct applying experimental and CFD approaches. In the air gap, the spent cooling air from rotor and stator meets and interacts with rotating and stationary geometries. Han et al., [2], Tang et al., [3] and Mayle et al., [4] investigated flow characteristics and thermal characteristics in the air gap for an air-cooled turbine generator using numerical and experimental methods. The end winding has complicated configuration connecting the stator bars in multiple locations. Tong [5] and Ujiie et al., [6] studied the flow field and heat transfer coefficient near end-winding using numerical method. Klomber et al., [7] propose correlations between the convective wall heat transfer coefficient and speed and flow rate parameters near end-winding region. Furthermore, the flow field near end-winding of hydrogenator for various ventilation scheme is reported [8]. The studies on the flow field of stator cooling system of hydrogenator was carried out by Carew and Freeston [9], and Schirittweiser [10]. They show that major parts of the total pressure losses occur near wedge region. Shuye [11], Guanbushanam et al., [12] and Pasha et al., [13] investigated hydraulic loss factor and overall pressure drop of stator ventilation ducts. There are also reports [14,15] on the detail pressure distribution on the stator ventilation ducts of hydrogenator, especially in the vicinity of stator bar. Li et. al., [16] investigated flow rate distribution of stator ventilation ducts by varying axial velocity at the entrance of air gap.

The present study focuses on evaluating the full surface heat transfer and pressure loss of stator ventilation ducts of air-cooled turbine generator. Since the most of heat is generated in the stator bar, its cooling system, so-called stator ventilation duct plays very important role to achieve the reliability and efficiency of a turbine generator. The real geometry and operating condition of the stator ventilation duct of an air-cooled turbine generator (200MVA) was modelled to investigate the characteristics of heat transfer and pressure loss experimentally and numerically. Annular section (24°) of stator ventilation duct is selected for modelling experiment and CFD analysis. The experimental rig is developed to simulate the radially (1) outward flow and (2) inward flow conditions. In addition, the (3) inward flow condition with cross flow is also investigated to represent the effect of the cross flow in the air gap. The full surface heat transfer distribution is measured by applying the transient heat transfer tests using thermochromic liquid crystals (TLC). A series of Computational Fluid Dynamics (CFD) analysis is also conducted to support the observation from the experiment.

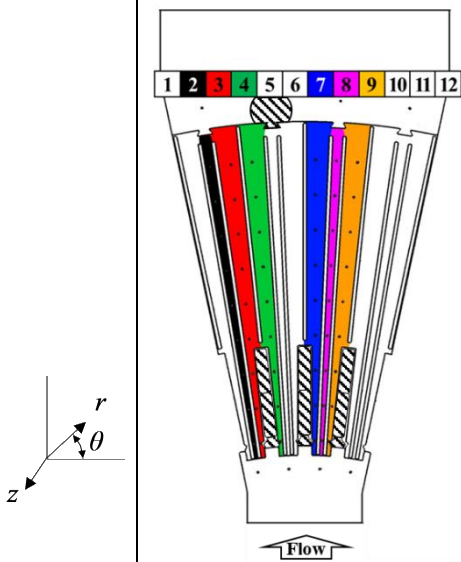
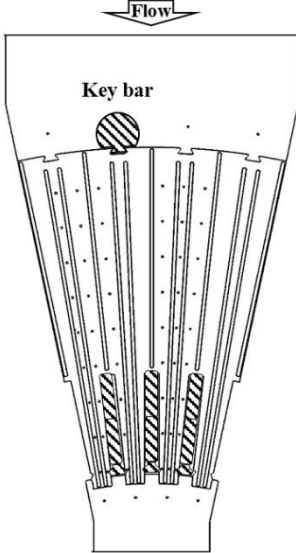
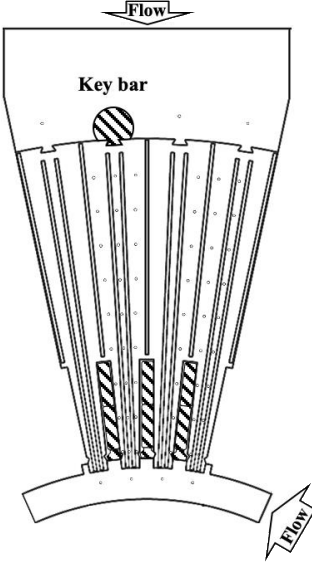
2. EXPERIMENTAL AND COMPUTATIONAL APPROACHES

2.1. Experimental Model and Approach

In the Table 1, the selected annual sector (24°) of the stator ventilation cooling system is shown. Referring to the model (1), the selected annular section includes four repeated passages. Each passage is divided into three individual ducts, so-called stator ventilation ducts. The middle duct

(2nd duct) has simple diffuser-shaped geometry ($\theta = 1^\circ$) as the cross-sectional area increases along the radial direction. The other two ducts are symmetric (for example, 3rd and 4th ducts, $\theta = 2^\circ$). The cooling air through these two symmetric ducts is in direct contact with the stator bar which is the main source of the heat due to the ohm loss. The wedge is to hold the position between stator bar and stator ventilation duct. It should be noted that the cross-sectional area is minimum at the wedge. The key bar installed in the end of 4th~6th ducts is to hold the stator ventilation ducts in axial direction. There are three different flow configurations to be tested: (1) Outward flow, (2) Inward flow and (3) Inward with cross flow as shown in Table 1. Those represent all possible flow conditions depends on the location of the stator ventilation duct (refer to **Error! Reference source not found.**).

Table 1. The details stator ventilation duct and real scale test models

Model	(1) Outward flow	(2) Inward flow	(3) Inward with cross flow
			

The 2nd and the 3rd ducts are selected for detailed analysis because those configurations are repeated geometries. Figure 2 shows the detail geometry of the ducts and its cross-sectional shape at each end. In addition, the two distinguishing geometric features, (a) wedge and (b) stator bar are shown in detail. In the 3rd duct, the wedge is located at $r/R \sim 0.11$ and the region of $0.11 < r/R < 0.3$ is in contact with stator bar. The variation of its cross-sectional area is shown in Figure 3. As noted, there are two abrupt changes in cross-sectional area of the 3rd duct due to the presence of wedge and stator bar. Contrary, the area variation of the 2nd duct is continuous as the radius increases.

To characterize the detailed heat transfer and pressure loss, the corresponding local Reynolds numbers are defined based on the inlet hydraulic diameter and aerothermal condition for each cooling flow direction. However, the average Reynold numbers were used to compare the overall heat transfer and pressure loss values. In **Error! Reference source not found.**, local and average Reynold numbers were reported as the test matrix.

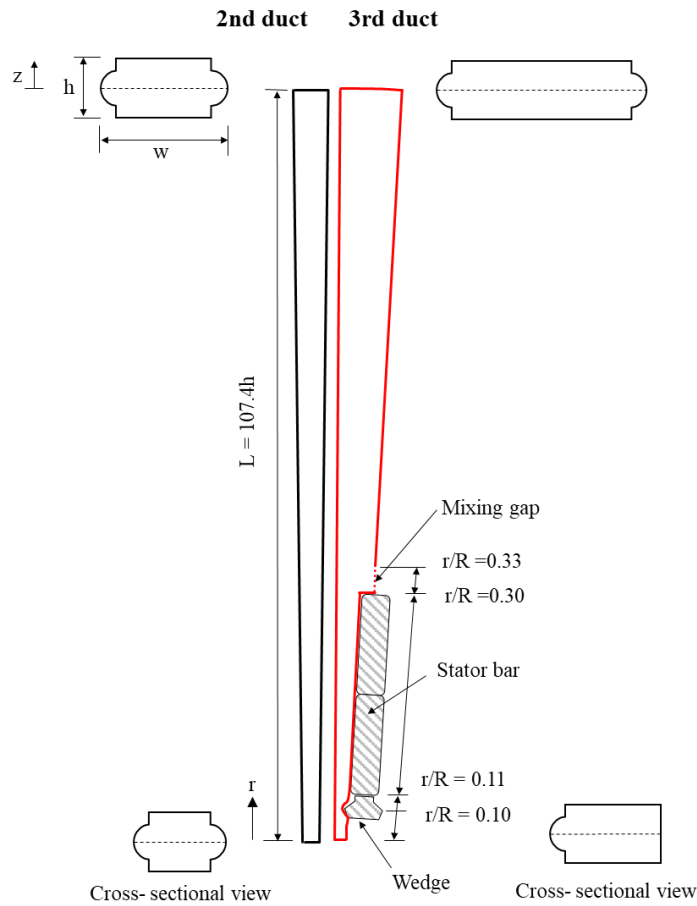


Figure 2. The geometrical details of the stator ventilation ducts (plane and cross-sectional views)

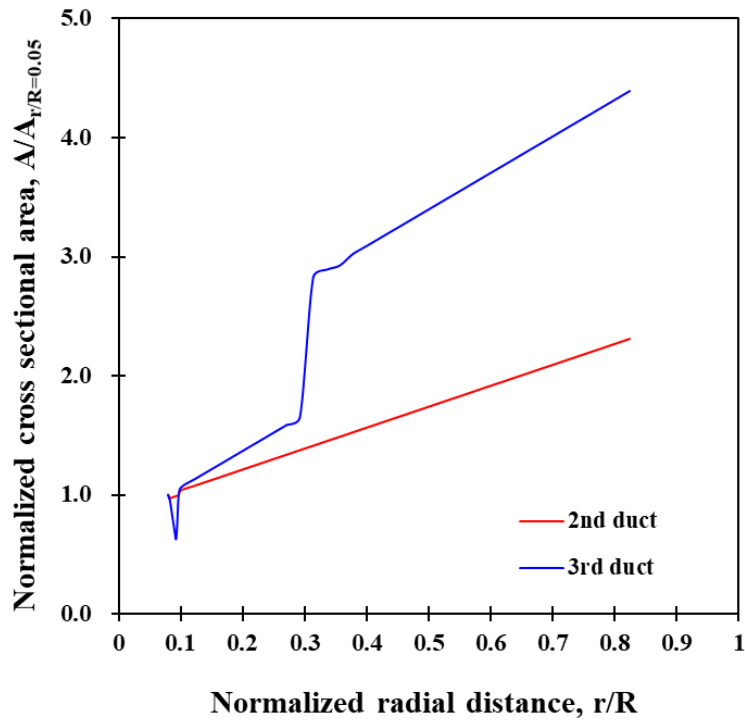


Figure 3. The variation in the cross-sectional area of the 2nd and 3rd ducts

Table 2. Test matrix and Reynold numbers based on inlet as well as average hydraulic diameters.

Duct type	Re	Outward flow			Inward flow			Inward with cross flow		
2nd duct	Re _{in}	11671	13817	18805	10157	13179	18983	10569	14083	17894
	Re _{avg}	14689	17391	23669	8425	10933	15747	8767	11683	14844
3rd duct	Re _{in}	17602	20807	27774	5159	6785	9520	5573	7452	9460
	Re _{avg}	27151	32095	42842	3816	5020	7043	4123	5513	6998

Re_{in} and Re_{avg} are representing the Reynolds numbers based on inlet hydraulic diameter and average hydraulic diameter, respectively.

The schematics of the test facility including pump, orifice, honeycomb, test model with bell mouth is shown in Figure 4. For the experiment, a real scale model is made from Perspex. The detailed heat transfer is measured applying thermochromic liquid crystals to the internal surfaces of stator ventilation ducts. A fast response heater mesh developed by Gillespie [17] and Gillespie et. al [18] is used to provide the step change in air temperature at the inlet of the test model.

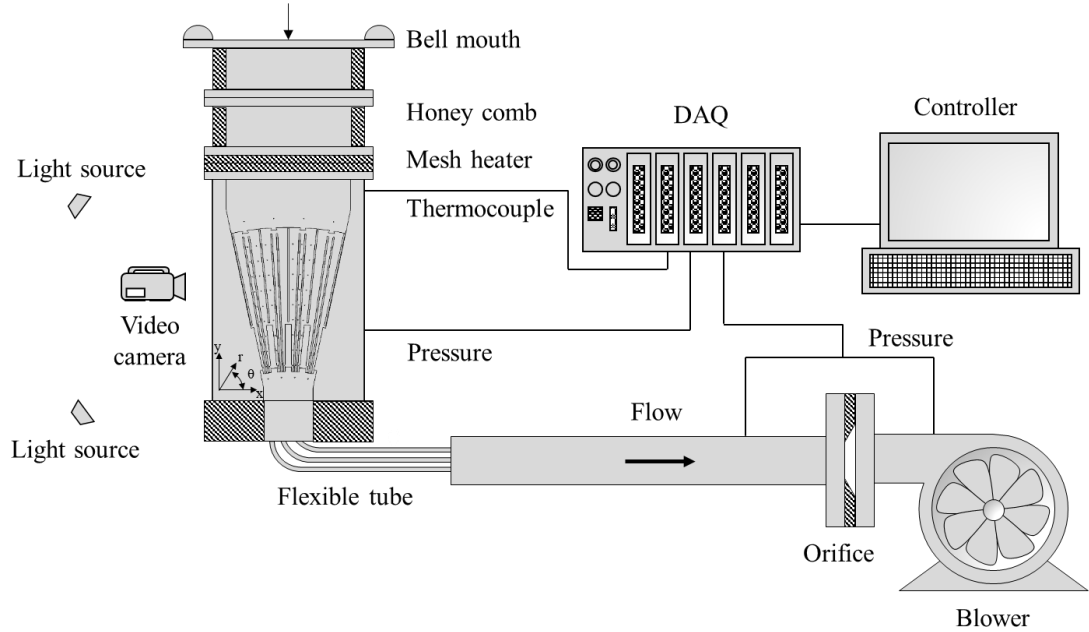


Figure 4. Schematic of test facility (set-up for inward flow)

A data acquisition system records all of the thermocouple and other voltage channels during the experiment. The system is capable of logging 32 channels at a sampling rate of 250 Hz. A program written in National Instrument LabVIEW 2009 controls the data acquisition hardware and allows the temperature and voltage measurements. The upstream and downstream pressure differences across the orifice flow meter [19] were measured using pressure transducers (SENORTECHNICS, HDI Series). All pressure transducers were calibrated using a pressure calibrator (FLUKE, 718 1G). The same pressure transducers were also used to measure the local static pressure of the stator ventilation duct.

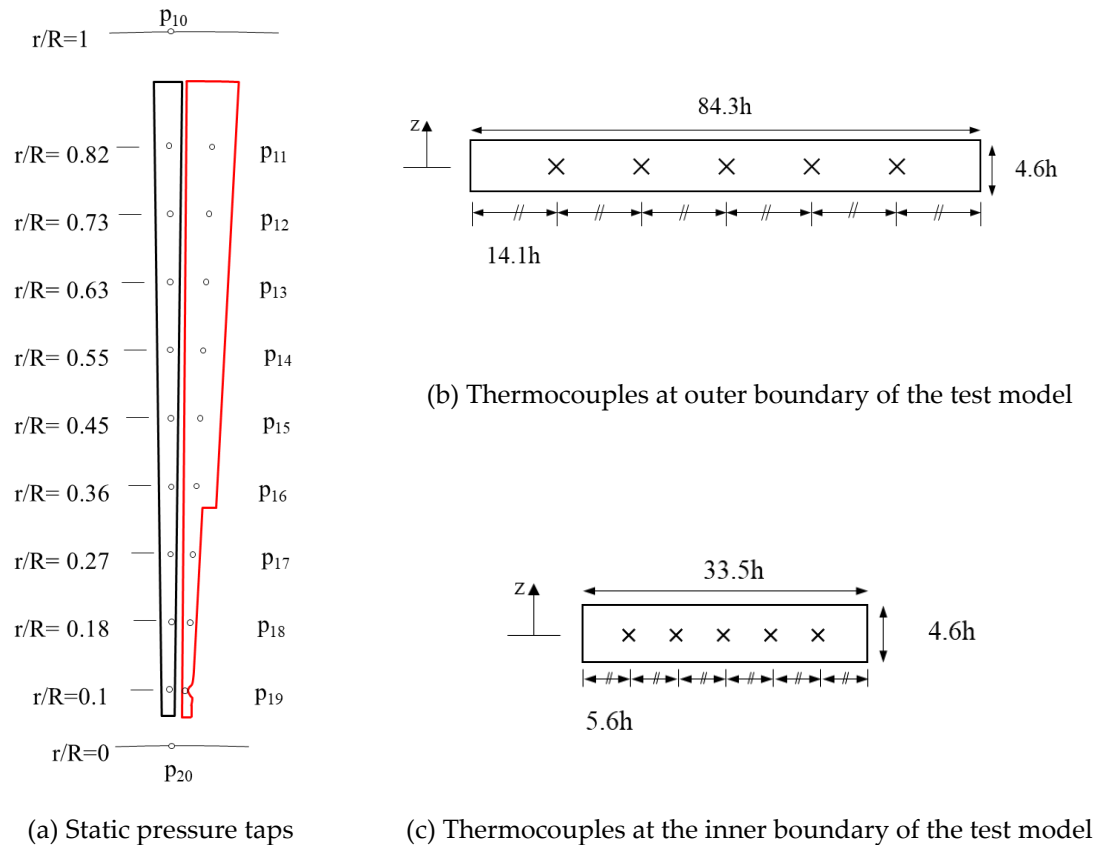


Figure 5. The measurement locations of static pressure and temperature

The local static pressure distributions of the stator ventilation ducts were measured using the radially distributed pressure taps. Figure 5 (a) shows the radial coordinates of ten pressure taps. Air temperature signals were recorded at two measurement planes. The positions of the air thermocouples are also shown in Figure 5 (b) and (c), respectively. The thermocouples (T-type) were calibrated against an RTD sensor (Omega, PT100 RTC Probe) using a temperature calibrator (Beames, MC5). Typical junction bead diameter is about 0.3 mm (Davidson and James [19]).

Transient heat transfer technique using thermochromic liquid crystals (TLC) are applied to measure fill surface heat transfer distribution. The experimental technique is well developed over decades and documented [1, 21–23]. The one-dimensional semi-infinite heat conduction equation was used to evaluate the local surface temperature; suitable boundary conditions must be applied for the heat conduction model to be valid [24]. The entire model must be isothermal at the beginning of each test to satisfy the boundary condition. Thus, before each experiment, the test surface is allowed to settle to the unheated flow temperature to satisfy the isothermal condition. The test surface is exposed to heated flow with a near-step increase in temperature, which results in a monotonic increase in surface temperature. The heat must not penetrate the full depth of the test surface during the experiment to satisfy the semi-infinite solid assumption. The use of a material of low thermal diffusivity (α), e.g., Perspex, $\alpha = 1.0 \times 10^{-7} \text{ m}^2 / \text{sec}$, increases the test time and also limits the lateral conduction (Schultz and Jones [27]). Perspex is frequently used because it is optically clear and has accurately known thermal properties (Ireland et al., [28]). For the current test rig, a minimum thickness of Perspex of 15 mm is used. This implies a penetration time ($\tau_{\text{penetration}}$) through the thinnest point of the test surface of approximately 140 seconds. From the color change of TLC, the local surface temperature is inferred indirectly as the heat transfer coefficient value is searched. For each stator ventilation duct heat transfer experiment, the color change of TLC was recorded using three digital full HD video cameras (JVC-GZ-HD6KR). LEDs (Light Emitting Diodes) were connected to the heater mesh power supply to indicate the start of heating and to match the start time of each

camera. The uncertainty in measured heat transfer coefficient, $\pm 7.3\%$, was calculated according to the procedure proposed by Kline and McClintock [25] and Moffat [26].

2.2 Computational Approach

CFD model represents the computational domains of the test model is built using a commercial code, FLUENT 14.0. The computational domain and the detail of mesh (18M cells) are shown in Figure 6. The cell growth ratio was limited to 1.2 to avoid large jumps in cell size, which may deteriorate numerical diffusion. The boundary layer through which the heat is transmitted in convective heat transfer must be modelled accurately in the simulation. The height of the first element adjacent to the wall Δy should be as small as possible to minimize y^+ . A fine prism layer of 15 was generated to achieve a non-dimensional wall distance (y^+) below 1 to allow the validity of using the enhanced wall treatments with the chosen turbulence model in the solver, where the viscous sub-layer and buffer zone were discretized.

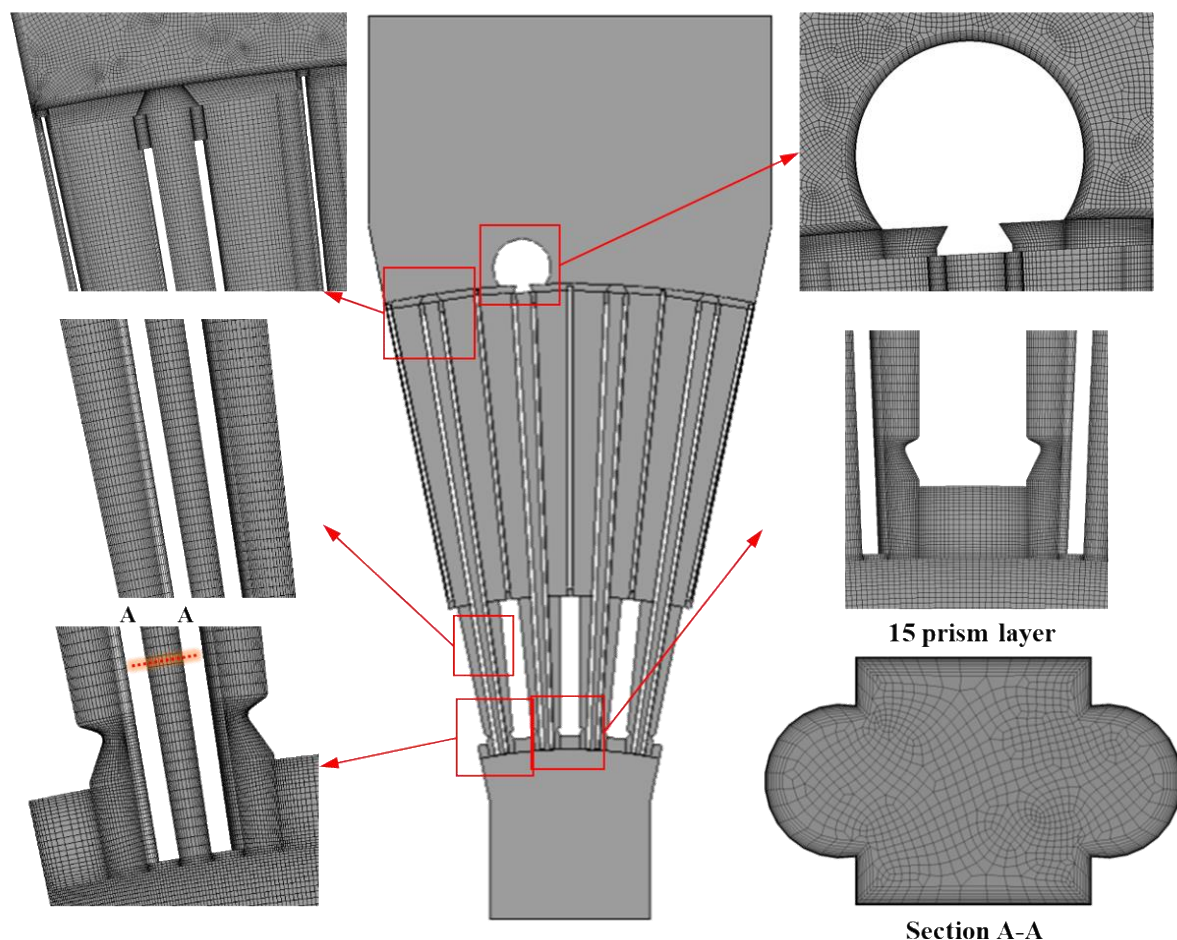
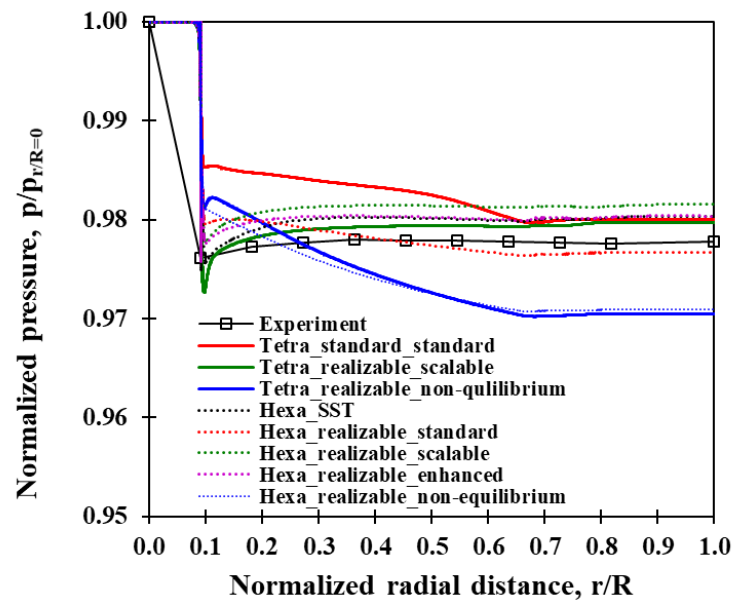


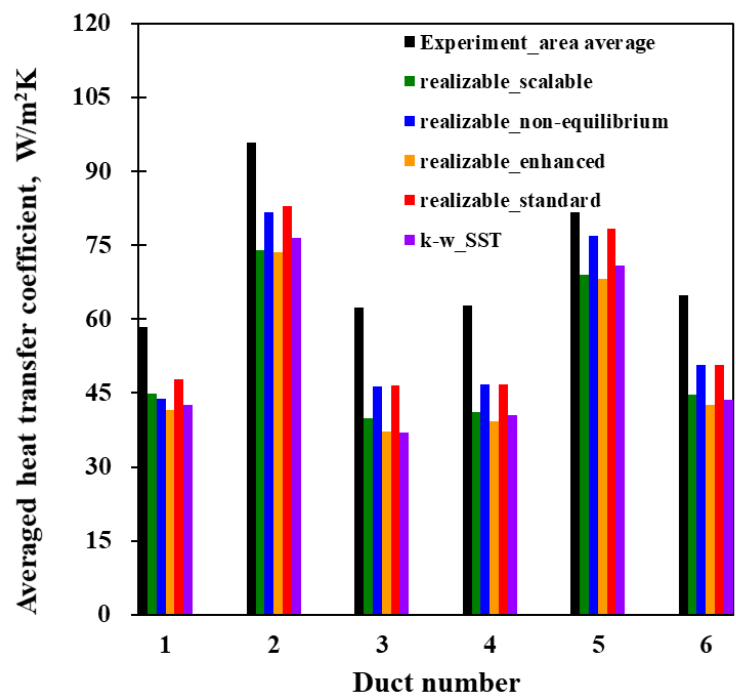
Figure 6. Computational domain and detail mesh

The Reynolds-averaged Navier-Stokes (RANS) equations are time-averaged equations to describe turbulent flows. The choice of the appropriate turbulence model has a major effect on the results. The comparison of various turbulence models is shown in Figure 7. It turns out that the $k-\varepsilon$ turbulence model with enhanced wall treatment fits best to the both pressure and heat transfer coefficient measurement results. Consequently, all simulations in this paper have been carried out using the $k-\varepsilon$ model with enhanced wall treatment.

For setting boundary conditions of the computation domain, the exact measurements made in the experiments are applied. Pressure inlet and outlet conditions are applied with constant wall temperature reflecting the transient heat transfer test condition.



(a) Mesh type and turbulence model sensitivity on the pressure distribution of the 2nd duct



(b) Turbulence model sensitivity using hexahedral mesh on the heat transfer distribution of the 2nd duct

Figure 7. Mesh type and turbulence model sensitivity study

3. RESULTS

3.1 Detailed Flow Filed Analysis

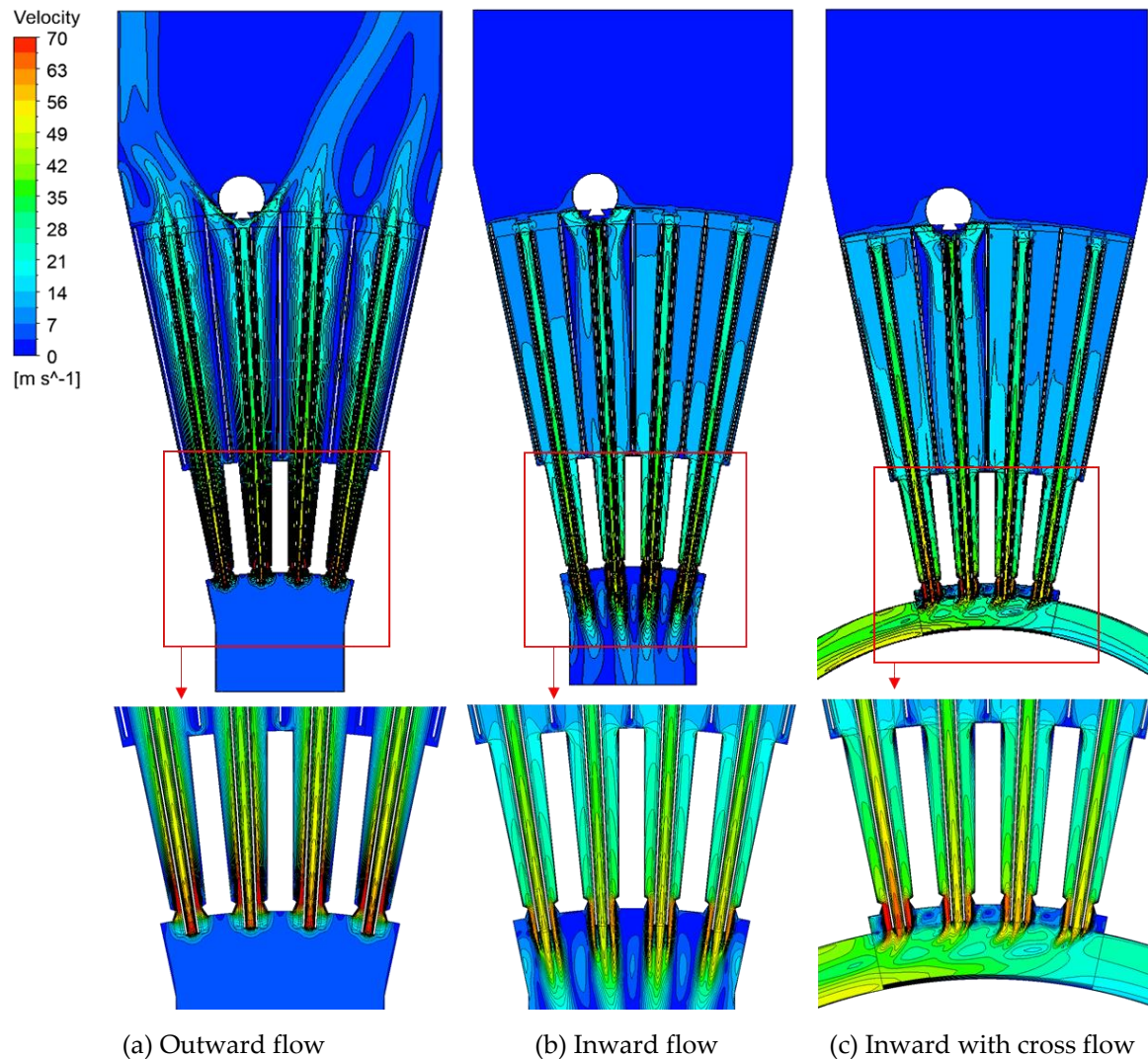


Figure 8. Comparison of velocity contours at $z/h=0.5$ plane

The velocity contours at mid height ($z/h=0.5$) are compared in Figure 8. It shows the characteristics of the three different cooling flow directions. In the comparison of inward and outward flow cases shown in Figure 8 (a) and (b), the clear distinction of the flow characteristics is observed at the inlet and exit of each case. The presence of key bar at the end of the 4th–6th ducts disturbs flow significantly and cause uneven flow distribution through the stator ventilation system. The effect of the cross flow can be clearly seen in Figure 8 (c). The cross flow represents the condition in air gap where the spent air from rotor and stator ventilation ducts interacts. Typical flow regime under the boundary condition is known as Taylor-Couette system. However, the circumferential velocity is dominant due to the high rotational speed and larger diameter of the rotor. Therefore, introducing the cross flow represents the realistic condition in the region. Since the model only represent an annular section (24°), the effect of the cross flow varies as it interacts with the spent air from the stator ventilation ducts. It also influences the heat transfer distribution.

For more detailed observation of the flow characteristics, the local velocity profiles are presented in Figure 9. The h is representing the height of the duct, which is constant along the radial direction while the width of duct, w is varying (refer to Figure 2). Each axis of the plot is normalized by the value at $r/R = 0.05$ which is the very beginning of the stator ventilation ducts. In comparison of outward and inward flow cases of the 2nd duct (Figure 9 (a), (b) versus (c), (d)), flow deceleration and acceleration depend on its flow direction are clearly observed. When the cross flow is

introduced to the inward flow case, Figure 9 (e) shows the distorted velocity profile at the exit plane of the 2nd duct ($r/R = 0.05$) as it was shown in Figure 8 (c). The velocity profiles in the 3rd duct, Figure 9 (f), (g) and (h), look more complicated as it is influenced by the variation in the cross-sectional area (refer to Figure 3). Compare to the 2nd duct (Figure 9 (b)), the peak velocity (at $r/R = 0.09$) of the 3rd duct of outward flow case (Figure 9 (f)), is about 3.5 times higher so that it results the higher dynamic head loss at the entry region as shown in Figure 10 (b). For the inward flow case of the 3rd duct, the peak velocity occurs at the exit, $r/R = 0.05$ and the similar distorted velocity profile is observed by introducing the cross flow, Figure 9 (g) and (h).

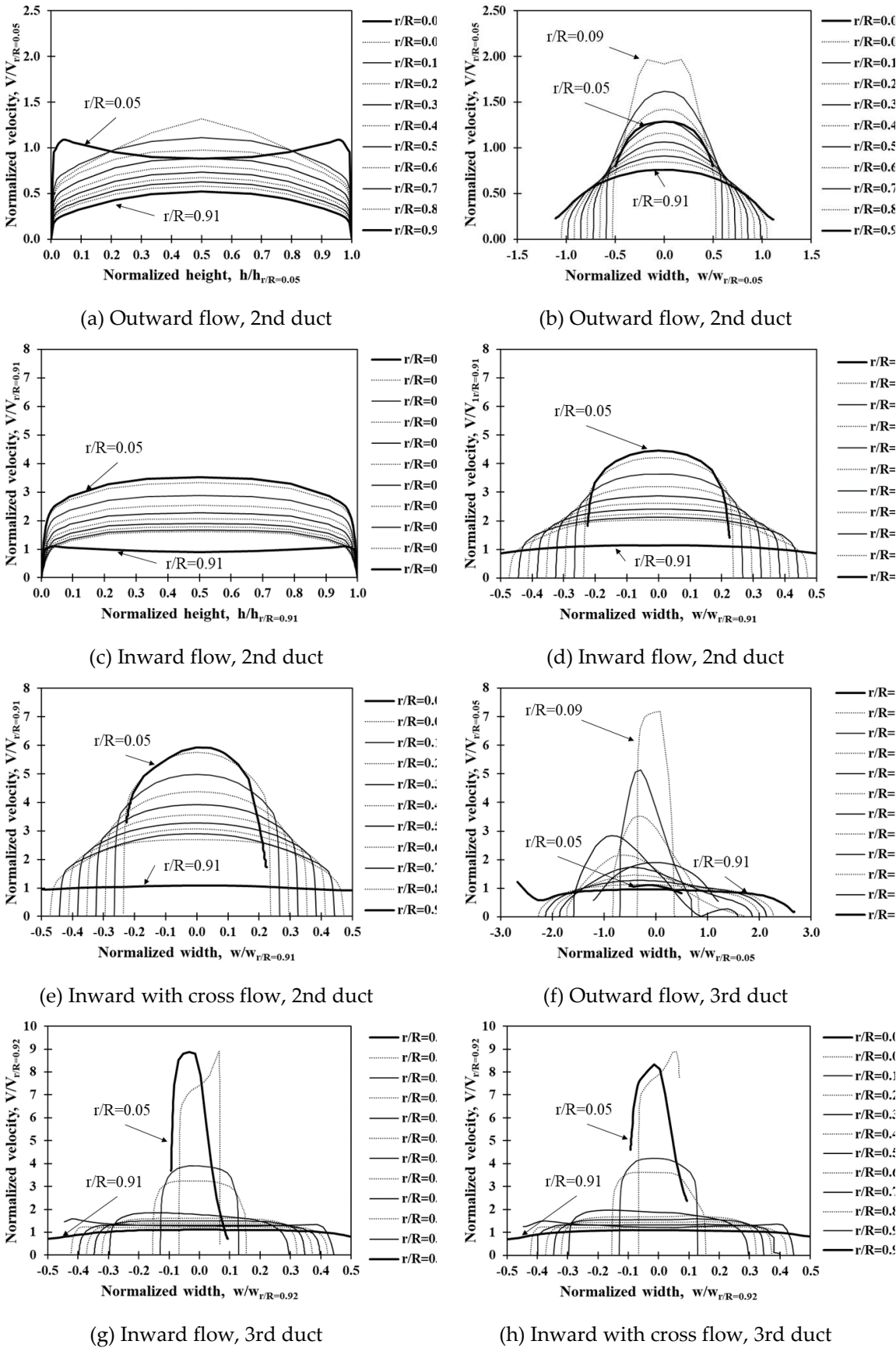


Figure 9. Comparison of local velocity profiles

3.2 Local Static Pressure Distribution

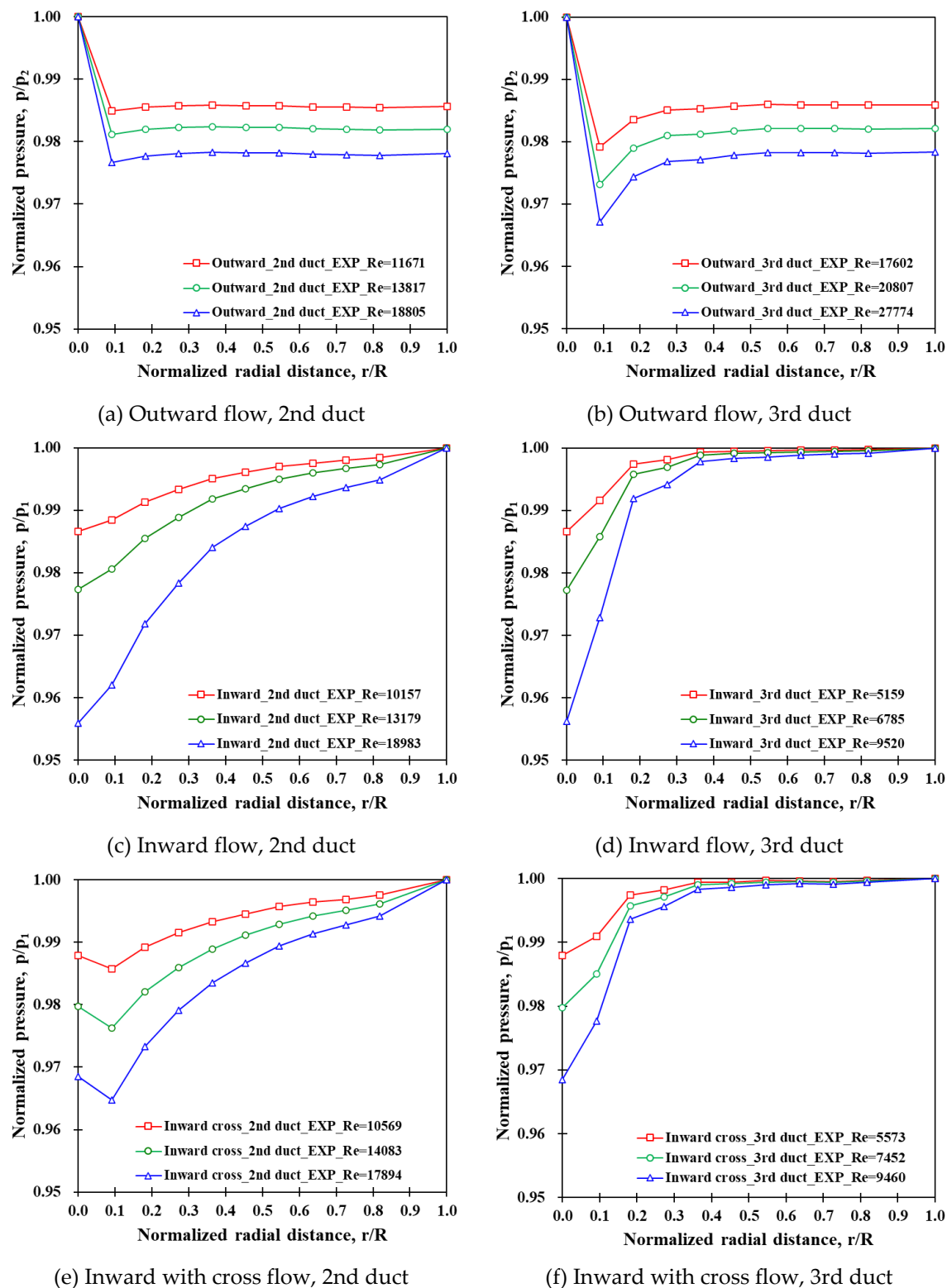


Figure 10. Comparison of local static pressure distribution

Figure 10 shows the local static pressure distributions of the 2nd and 3rd ducts. The radial locations of the static pressure taps are shown in Figure 5. The local static pressure is normalized by inlet static pressure at $r/R = 0$ or 1 depends its flow direction. For outward case, the 2nd and 3rd ducts can be considered as a diffuser. Therefore, local static pressure will be recovered while there is still frictional loss due to the effect of viscosity. In Figure 10 (a) and (b), it is observed that the

most of the pressure loss is occurring at the entrance region of the two ducts. The 3rd duct has a wedge soon after the sharp edge inlet region, resulting in higher pressure loss than the 2nd duct. In addition, there is also the stator bar which occupies the region of $0.11 < r/R < 0.3$. As the results, the full recovery of local static pressure is observed in the downstream of the region.

For the same 2nd and 3rd ducts, there is change in flow direction so that the Figure 10 (c) and (d) shows the local static pressure distribution of the inward cases. Now the two ducts can be regarded as a nozzle or a contracting duct. The flow velocity will be accelerated as the cross-sectional area decreases with no adverse pressure gradient. In the 3rd duct (Figure 10 (d)), the effect of abrupt change in the cross-sectional area is clearly shown in the region of $0.11 < r/R < 0.3$. Flow velocity will be accelerated further in the region which can cause sudden increase in pressure loss. After the entrance, flow passes the wedge region where the cross-sectional area is minimum so that the most of the pressure drop is occurring.

Introducing the cross-flow, the difference in local static pressure distribution of inward flow cases can be observed in the Figure 10 (e) and (f). The local static pressure in the exit region is influenced by cross flow which reflects the effect of the rotating flow in the air gap between the rotor and stator. For the 3rd duct, the accelerated flow velocity due to the wedge, prevent such a cross flow ingestion. The recognizable difference is seen in the exit region of the 2nd duct where the recovery of local static pressure can be observed.

3.3 Overall Frictional Loss (exclude entrance effect)

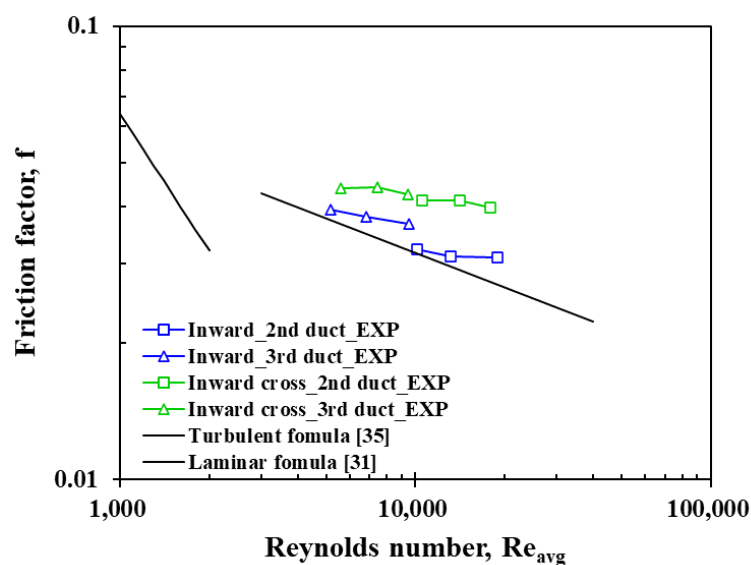
Figure 11 shows the friction factor distribution of outward flow, inward flow and inward with cross flow cases. The friction factor is calculated from the static pressure difference (excluding entrance effect), $\Delta p = p_{19} - p_{11}$ for outward flow case, $\Delta p = p_{11} - p_{19}$ for inward and inward with cross flow cases as

$$f = \Delta p \frac{D_h}{R} \frac{2}{\rho v^2} \quad (1)$$

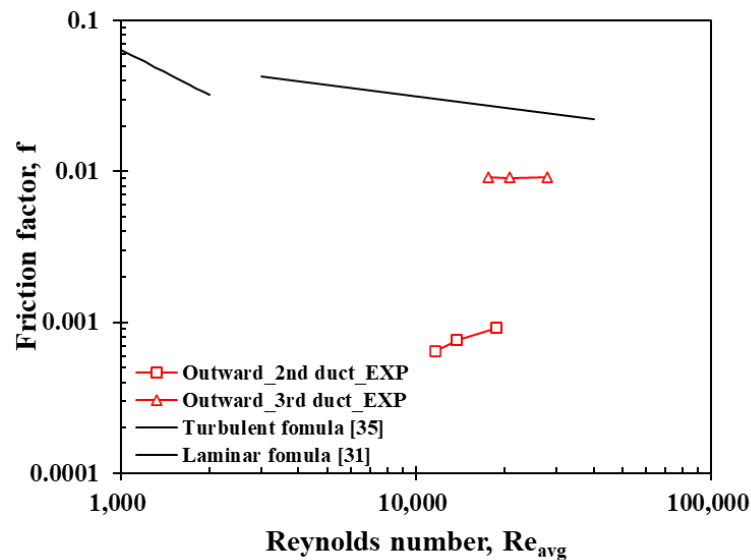
where, ρ is density; D_h is average hydraulic diameter; R is the radial distance of pressure measurement locations (p_{19} and p_{11}); v is inlet velocity.

f from the Blasius formula [31, 35] for turbulent flow in smooth pipes with $4 \times 10^3 < Re_{D_h} < 10^5$ is shown in the results for a reference.

$$f = \frac{0.316}{Re_{D_h}^{1/4}} \quad (2)$$



(a) Friction factor of inward flow and inward with cross flow cases



(b) Friction factor of outward flow case

Figure 11. Comparison of Friction factor (exclude entrance effect)

As the flow of the inward, and the inward with cross flow case continuously accelerates, the effect of frictional pressure loss is higher than the Blasius formula. The effect of cross flow to the friction factor is clearly seen in the comparison. For the outward flow case, Figure 11(b), the friction factor of the 2nd and 3rd ducts are much lower than Blasius formula as it behaves as a diffuser.

3.3 Heat Transfer Characteristics

Figure 12 shows the detailed Nusselt number distribution of outward case at three different Reynold numbers. The highest Nusselt number values are observed in the entrance regions as expected. In the entrance region of the 3rd duct, there is a wedge which has minimum cross-sectional area. Therefore, it suppresses the flow through the duct while there is no such a restriction in the 2nd duct. It results the difference in the comparison of Nusselt number distributions of the two ducts: the Nusselt number of the 3rd duct decreased rapidly through the stator bar region ($0.11 < r/R < 0.30$). The detailed Nusselt number distributions of inward case is presented in Figure 13. It shows the highest heat transfer in the entrance regions of the 2nd and 3rd ducts. Especially for the 3rd duct, higher heat transfer region around the stator bar ($0.11 < r/R < 0.30$) is observed. It is due to the accelerated flow around the stator bar as the cross-sectional area decreases. For the same reason, higher heat transfer region is shown in the downstream of the wedge. For the 2nd duct, as it has a nozzle-like geometry, the heat transfer increases smoothly as the flow accelerates. The detailed Nusselt number distribution of the inward with cross flow case is similar to the inward flow case as shown in Figure 14. The heat transfer coefficient of the second duct gradually decreases along the flow direction, while the that of the third duct has a peak value in the wedge region ($r/R = 0.1$). The peak heat transfer is due to the thin thermal boundary layer at the beginning of the entrance. Then, the heat transfer coefficient decays rapidly as the thermal boundary layer develops toward the downstream. The predicted heat transfer values from CFD show good alignment with the measurements.

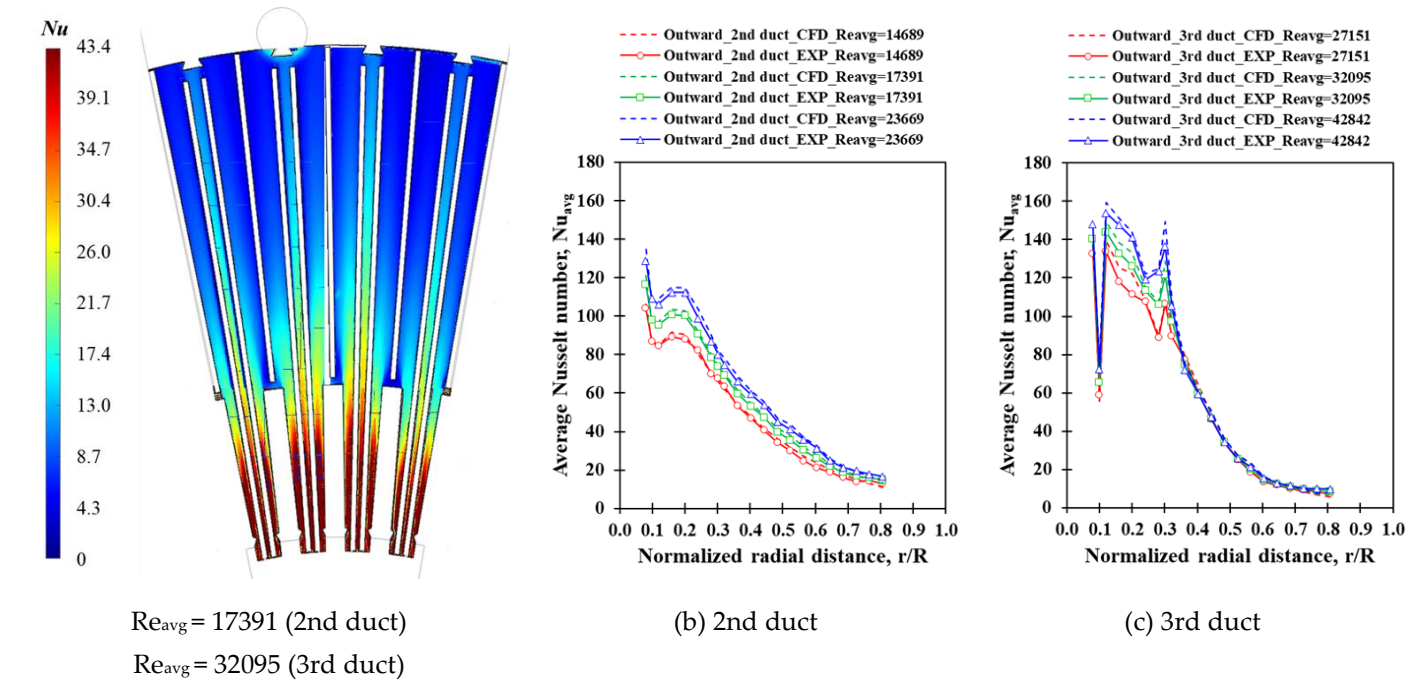


Figure 12 Nusselt number distribution of outward flow case

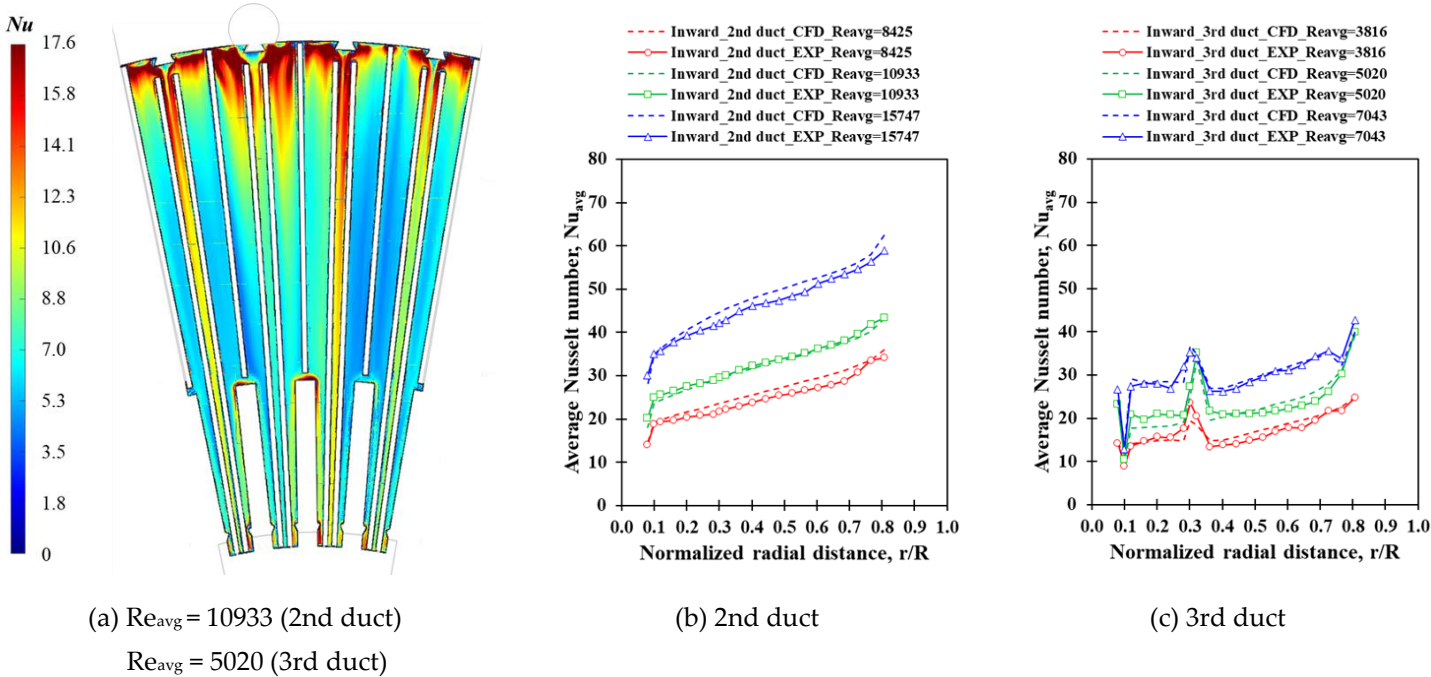


Figure 13 Nusselt number distribution of inward flow case

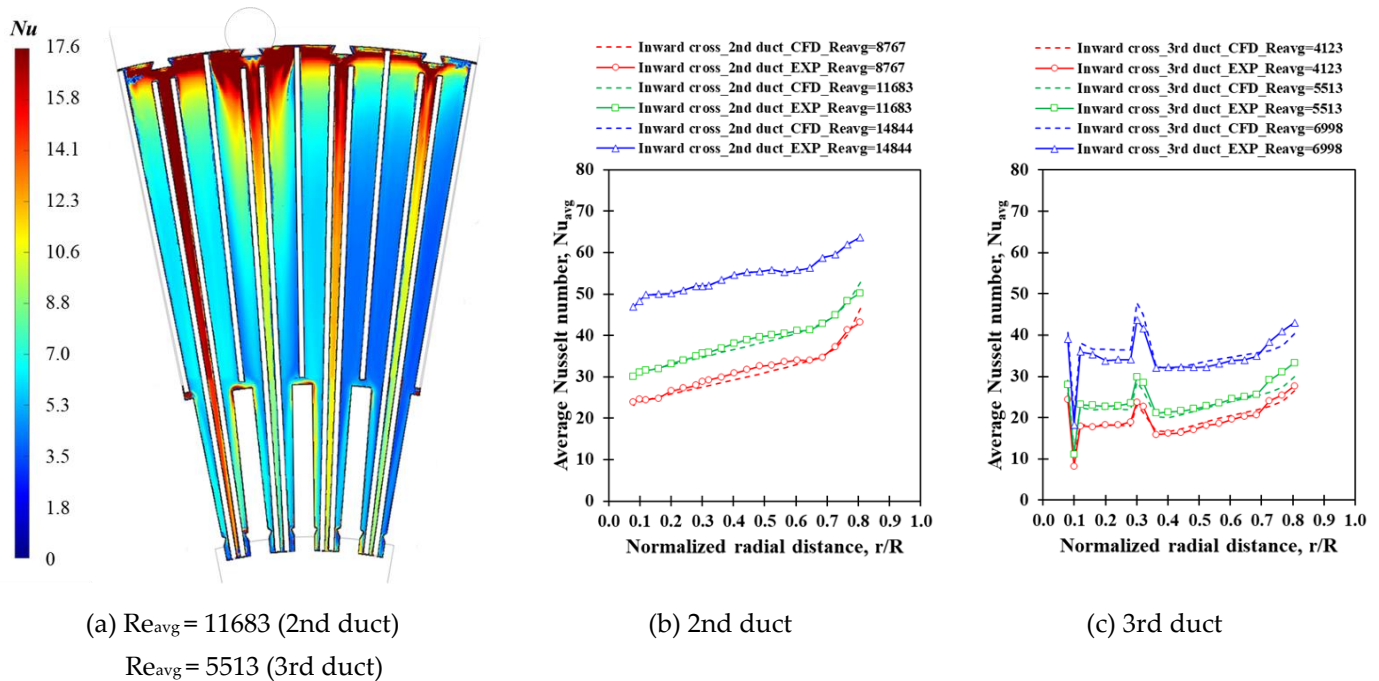


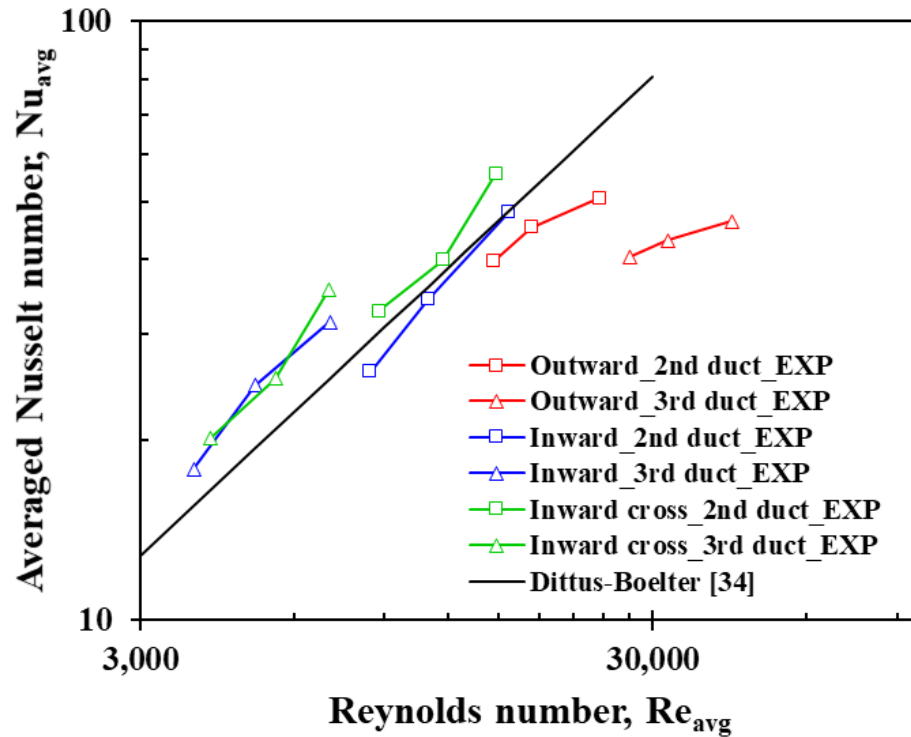
Figure 14. Nusselt number distribution of inward with cross flow case

3.5 Overall Area Averaged Heat Transfer

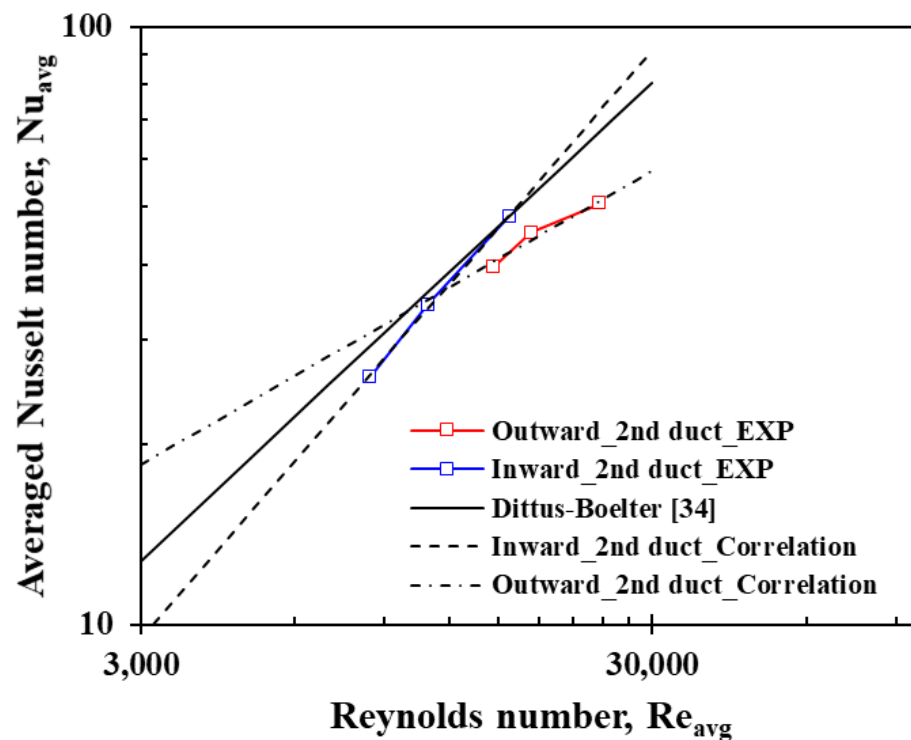
Figure 15 shows the comparison of overall area averaged Nusselt number. The trend of the outward flow case (Figure 15 (a)) shows different gradient compare to the inward and inward with cross flow cases. The effect of the cross flow is more dominant for the 2nd duct compare to the 3rd duct values. It is mainly because of the abrupt changes in local heat transfer due to the wedge and stator bar of the 3rd duct. In addition, toward the downstream of stator bar ($r/R > 0.3$), the local heat transfer distribution of the 3rd duct is very sharply decreasing as shown previously in Figure 12 (a). Because of no interference and a constant decreasing cross-sectional area, the flow through the 2nd duct accelerates so that exhibits higher heat transfer than the Dittus-Boelter correlation. For the outward flow case, the cross-sectional area is increasing in the radial direction. As the result, flow decelerates so that it does not promote heat transfer. While there was no useful reference to compare the heat transfer, Dittus-Boelter correlation (Equation 3) was added for reference.

$$Nu_{DB} = 0.243Re^{0.8}Pr^{0.4} \quad (3)$$

where, Pr is Prandtl number.



(a) Overall area averaged Nusselt number



(b) Nusselt number correlations of the 2nd duct

Figure 15. Comparison of overall area averaged Nusselt numbers

Since the heat transfer correlation representing the stator ventilation duct (wedge-shaped duct) is rarely available, it will be worthwhile to report the experimental correlations from the present work. The equation (4) and (5) are the new correlations based on the outward and inward flow cases of the 2nd duct. Depends on flow directions, each case represents the heat transfer in a simple

diffuser or nozzle geometry with angle of 1° . The comparison among the measured data, new correlations and Dittus-Boelter correlation is shown in Figure 15 (b).

$$\text{Inward flow correlation} \quad Nu_{\theta=1^\circ} = 0.00413 Re_{avg}^{0.98} Pr^{0.4} \quad (4)$$

$$\text{Outward flow correlation} \quad Nu_{\theta=1^\circ} = 0.4145 Re_{avg}^{0.49} Pr^{0.4} \quad (5)$$

4. CONCLUSION

This paper presents experiments and CFD analysis to investigate the full surface heat transfer coefficient and pressure loss characteristics of stator ventilation duct of a turbine generator. Real scale models are developed for the present study. The measured heat transfer and pressure data is used to selected promising mesh type and turbulence model for CFD prediction. The sensitivity study will be useful guideline for other researchers. The predicted velocity profiles using the validated CFD model provide insight to understand the pressure loss and heat transfer mechanism observed from the measured data. Since the model represent a real geometry, there was strong entrance effect on the velocity profile and local static pressure distribution of all cases. The effect of cross flow reduces average heat transfer as it builds extra pressure in the mixing zone. These findings are also observed from the measured full surface heat transfer distributions. For the inward case, the results suggest that the average Nusselt number of the 2nd duct is about 30% higher than the 3rd duct. The trend is similar with the effect of cross flow. For the outward flow case, the average Nusselt number of the 2nd duct is also higher than the 3rd duct.

To the best of authors' knowledge, the present results are the first reported data on full surface heat transfer coefficient of stator duct ventilation duct. Hence the findings and proposed new correlation will be useful reference for future study.

Author Contributions: Conceptualization, Shinyoung Jeon and Changmin son.; methodology, Shinyoung Jeon; software, Shinyoung Jeon; validation, Shinyoung Jeon; formal analysis, Shinyoung Jeon and Changmin son; investigation, Shinyoung Jeon and Changmin Son; resources, Shinyoung Jeon; data curation, Shinyoung Jeon; writing—original draft preparation, Shinyoung Jeon; writing—review and editing, Shinyoung Jeon and Changmin Son; visualization, Shinyoung Jeon; supervision, Changmin Son; project administration, Changmin Son; funding acquisition, Changmin Son.

Funding: The authors would like to thank Doosan Heavy Industries & Constructions for their support and technical guidance. Furthermore, this work was supported by the Korea Institute of Energy Technology Evaluation and Planning (KETEP) and the Ministry of Trade, Industry & Energy (MOTIE) of the Republic of Korea (No.20181110100400).

Conflicts of Interest: The authors declare no conflict of interest.

References

1. Yoo, W., Jeon, S., Son, C., Yang, J., Ahn, D., Kim, S., Hwang, K. and Ha, S., Full surface heat transfer characteristics of rotor ventilation duct of a turbine generator, *Applied Thermal Engineering*, 2016, 94, pp.385-394.
2. Han, J.D., Hong, G.Y., Tang, L. and Lu, Y.P., Numerical studies on the flow field of stator and air gap for large air-cooled turbo-generator. In *Advanced Materials Research*, 2012, Vol. 516, pp. 970-975.
3. Tang, L., Lu, Y.P., Deng, H.Y. and Wang, Z.M., Research of Flow Field and Temperature Field in 2D Annular Space of Air-Gap, In *Applied Mechanics and Materials*, 2012, Vol. 214, pp. 76-81.
4. Mayle, R.E., Hess, S., Hirsch, C. and Van Wolfersdorf, J., Rotor-stator gap flow analysis and experiments. *IEEE transactions on energy conversion*, 1998, 13(2), pp.101-110.
5. Tong, W., 2008. Numerical analysis of flow field in generator end-winding region. *International Journal of Rotating Machinery*, 2008.

6. Ujiie, R., Arlitt, R. and Etoh, H., Application of computational fluid dynamics (CFD) on ventilation-cooling optimization of electrical machines. Review Energy Technologies-generation, transmission and distribution of electric and thermal energy (ICEMENERG), 2006, pp.17-22.
7. Klomberg, S., Farnleitner, E., Kastner, G. and Bíró, O., Characteristics of the Convective Heat Transfer Coefficient at the End Winding of a Hydro Generator, *Proceedings of the ASME 2013 Power Conference*, 2013, POWER2013-98093.
8. Klomberg, S., Farnleitner, E., Kastner, G. and Bíró, O., Numerical Study of the Cooling Air Flow in a Hydro Generator with Various Ventilation Scheme, *11th International World Congress on Computational Mechanics (WCCM XI)*, 2014, pp. 1-2.
9. Carew, N. J. and Freeston, D. H., Fluid Flow Losses in A. C. Generator Stator Ventilation Ducts, *Proceedings of the Institution of Mechanical Engineering conference Proceedings*, 1967, Vol. 182, No. 4, pp. 87-95.
10. Schirittweiser, M.m Marn, A., Farnleitner, E. and Kastner, G., Numerical Analysis of Heat Transfer and Flow of Stator Ducts Model, *IEEE Transactions on Industry Applications*, 2014, Vol. 50, No. 1, pp. 226-233.
11. Shuye, D., Haoran, L., Zhaoqiong, S. and Yunzhong, G., Research of Fluid Flow Characteristic inside Radial Ventilation Duct for Large Generator, *Power and Energy Engineering Conference (APPEEC)*, 2010, pp. 1-4.
12. Gunabushanam, N. and Suresh, J. V., Experimental and CFD Analysis of Hydrogenerator Ventilation Components, *CIGRE 2006*, 2006, pp. 1-7.
13. Pasha, A. A., Hussain, M. and Gunubushanam, N., Experimental and CFD Analysis of Hydrogenerator Stator, *Proceedings of the 37th National & 4th International Conference on Fluid Mechanics and Fluid power*, 2010, FMFP10-EM-14.
14. Rao, G. C., Rajulu, K. G., and Gunabushanam, N., Design and Analysis of Hydro Generator Ventilation System using Experimental and CFD, *World Academy of Science, Engineering and Technology*, 2011, Vol. 51, pp. 277-280.
15. Gregorc, B., Investigating the Malfunction of a Hydrogenerator's Cooling-System, *TMT 2011 15th International Research/Expert Conference, Trends in the Development of Machinery and Associated Technology*, 2011.
16. Li, Y., Li, W. and Su, Y., Sensitivity of Axial Velocity at the Air Gap Entrance to Flow Rate Distribution at Stator Radial Ventilation Ducts of Air-Cooled Turbo-Generator with Single-Channel Ventilation, *Energies*, 2019, 12(18), p. 3442.
17. Gillespie, D. R. H., Intricate Internal Cooling Systems for Gas Turbine Blading, D.Phil. Thesis, Department of Engineering Science, University of Oxford, 1996.
18. Gillespie, D. R. H. and Ireland, P. T., "Heating Element," Patent No:US6181874
19. BS EN ISO 5167-2, Measurement of Fluid Flow by Means of Pressure Differential Devices Inserted in Circular Cross-section Conduits Tuning Full – Part 2: Orifice Plates (ISO 5167-2:2003), ISBS 0 580 4145 6, 2003.
20. Davidson, S. R. H. and James, D. F., Measurement of thermal conductivity of bovine cortical bone, *Medical Engineering & Physics*, 2000, Vol. 22, pp. 741-747.
21. Gillespie, D. R. H., Wang, Z., Ireland, P. T. and Kohler, S. T., Full surface local heat transfer coefficient measurements in a model of an integrally cast impingement cooling geometry, *Journal of turbomachinery*, 1998, vol. 120(1), pp.92-99.
22. Park, N., Son, C., Yang, J., Lee, C. and Lee, K., Full Surface Heat Transfer Measurement of a Turbine Internal Cooling System Using a Large Scaled Model, 2018, ASME Paper No. GT2018-77218.
23. Song, I., Son, C., Yang, J., Lee, C. and Lee, K., Thermal Performance of the Realistic Leading Edge Cooling Passage of a Turbine Blade, 2018, ASME Paper No. GT2018-77217.
24. Clifford, R. J., Jones, T. V. and Dunne, S. D., Techniques for Obtaining Detailed Heat Transfer Coefficient Measurements Within Gags Turbine Blade and Vane Cooling Passage, 1993, ASME paper 83-GT-58.
25. Kline, S. and McClintock, F., Describing Uncertainties in Single-Sample Experiments, *Mechanical Engineering*, 1953, Vol. 75, pp. 3-8.
26. Moffat, R.J., Describing the uncertainties in experimental results, *Experimental thermal and fluid science*, 1988, Vol. 1(1), pp.3-17.

27. Schultz, D. L. and Jones, J. V., Heat Transfer Measurements in Short-Duration Hypersonic Facilities, 1973, AGARD-AG165.
28. Ireland, P. T., Wang, Z. and Jones, T. V., Measurement Techniques, von Karman Institute for Fluid Dynamics, Lecture Series 1994-1995, 1995.
29. Jeon, S., A Study on the Cooling Performance of a Turbine Generator Stator Ventilation Duct System, Master Thesis, School of Mechanical Engineering, Pusan National University, Republic of Korea, 2015.
30. Gibson, A. H., On the Flow of Water through Pipes and Passages having Converging or Diverging Boundaries, *Proceedings of the Royal Society of London, Series A, Containing Papers of a Mathematical and Physical Character*. 1910, Vol. 83, No. 563, pp. 366-378.
31. Munson, B. R., Young, D. F., Okiishi, T. H. and Huebsch, W. W., Fundamentals of Fluid Mechanics, John Wiley & Sons, Inc. pp.415, 2006.
32. Dittus, F. W., and Boelter, L. M. K., Heat Transfer in Automobile Radiators of the Tubular Type, *University of California Publications in Engineering*, 1930, Vol.2, pp. 443-461.
33. Tsang, C. L. P., High Blockage Turbulators in Gas Turbine Cooling Passage, D.Phil. Thesis, Department of Engineering Science, University of Oxford, UK, 2002.
34. Metzger, D. E. and Larson, D. E., Use of Melting Point Surface Coating for Local Convection Heat Transfer Measurement in Rectangular Channel Flows with 90-deg Turns, *Journal of Heat Transfer*, 1986, vol. 108(1):48-54.
35. Blasius, H., 1913. Das aehnlichkeitsgesetz bei reibungsvorgängen in flüssigkeiten. In Mitteilungen über Forschungsarbeiten auf dem Gebiete des Ingenieurwesens (pp. 1-41). Springer, Berlin, Heidelberg.